Vol. 47, No. 4 (2025) 673-691, DOI: 10.24874/ti.1991.07.25.11

Tribology in Industry

www.tribology.rs

RESEARCH

Numerical Investigation of Slip Effects and Cavitation in Hydrodynamic Thrust Bearing with Circumferential Pocket Geometry

Imam Syafaat[a,*], Agung Nugroho[a], Nur Kholis[a], Muhammad Abdul Wahid[a], Helmy Purwanto[a], Riky Setiyanto[a], Santhi Wilastari[b], Muchammad Muchammad[c]

[a]*Department of Mechanical Engineering, Faculty of Engineering, Universitas Wahid Hasyim, Jl. Raya Gunungpati Nogkosawit KM.15, Nongkosawit 50225, Gunungpati, Semarang, Indonesia,*
[b]*Department of Ship Machinery Engineering Technology, Politeknik Bumi Akpelni, Jl. Pawiyatan Luhur II/17, Bendan Duwur 50235, Semarang, Indonesia,*
[c]*Department of Mechanical Engineering, Faculty of Engineering, Diponegoro University, Jl. Prof Sudarto SH Tembalang 50275, Semarang, Indonesia.*

Keywords:

Thrust bearing
Slip
Cavitation
Surface texture
CFD
Load-carrying capacity

* Corresponding author:

Imam Syafaat
E-mail: imamsyafaat@unwahas.ac.id

Received: 27 July 2025
Revised: 20 September 2025
Accepted: 3 November 2025

A B S T R A C T

The impact of cavitation on bearing performance is frequently overlooked in the scant research on textured bearings. This study investigates the load-carrying capacity of a thrust bearing under cavitation conditions with lubricant film thickness variations and circumferential pocket surface textures. This research's novelty consists on integrating texturing, cavitation, and slip engineering to evaluate load-carrying capacity. The slip conditions were implemented at various locations, including before the pocket, on the pocket, both before and on the pocket (combined), and without a slip as a reference. Computational fluid dynamics was used for the analysis in both cavitation and no cavitation scenarios. The results show that the highest maximum pressure, 5.09 MPa, was achieved with a 15 μm film thickness with slip applied prior to the pocket. When there was no slip, the lowest pressure was recorded at 80 μm film thickness. With the maximum load-carrying capacity of 1744.61 N, the slip-before-pocket arrangement continuously demonstrated superior performance across all configurations. In comparison to the cavitation scenarios, the no cavitation simulations produced superior pressure and load bearing capacities across all film thickness and slip changes.

1. INTRODUCTION

Hydrodynamic thrust bearings are a type of fluid film bearing crucial for sustaining axial loads in rotating machinery. The fundamental operational concept involves establishing a thin lubricating layer that separates the stationary (stator) and rotating (rotor) components, thereby preventing direct metal-to-metal contact. The lubrication layer is produced by hydrodynamic pressure, which occurs as the lubricant is pulled into a narrowing gap formed by the relative motion of surfaces. When sufficient velocity and lubricant availability are present, a pressure field is created that can support significant loads, significantly reduce friction, and reduce surface wear [1]. These bearings are crucial in high-load applications, such as power generation turbines, marine propulsion systems, and large-scale pumps employed in offshore and energy industries. Their reliability directly affects the overall effectiveness and durability of machinery. The load-carrying capacity (LCC) is a vital indicator of the performance of thrust bearings, intricately associated with the pressure distribution inside the lubricating film. Comprehensive studies have concentrated on innovations in surface design, lubricant management, and material selection to enhance efficiency and durability while reducing maintenance costs.

Surface texturing has emerged as a highly effective tribological technique for enhancing the performance of thrust bearings. Incorporating micro- or nano-scale features, such as dimples, grooves, or pockets, on the bearing surface helps control lubricant flow, improve hydrodynamic pressure accumulation, and reduce frictional resistance [2]. The textured regions serve as micro-reservoirs that preserve and disperse lubricant during operation, hence augmenting load capacity and reducing the likelihood of lubricant depletion. A large number of studies have demonstrated the effectiveness of surface texturing in improving tribological performance. Huang and Zhang [3] performed a computational analysis of inclined pad thrust bearing and discovered that surface roughness significantly influences hydrodynamic pressure and LCC, particularly with reduced lubricant clearances. Similarly, Yu et al. [4] developed a computational model that integrated square textures and cavitation events. Their findings revealed that modified texture dimensions enhanced LCC by over 19%, illustrating the considerable potential of engineered surface attributes to augment bearing reliability.

Experimental and numerical investigations [5-11] consistently indicate that texturing reduces friction and improves load support, especially under mixed or boundary lubrication conditions. The texturing design necessitates optimization. Shallow pockets or grooves can promote pressure buildup, whereas excessively deep texturing may trap cavitation bubbles or disrupt lubricant continuity, leading to reduced performance [12]. The form, distribution, and depth of textures require careful assessment to achieve the ideal balance between friction reduction and pressure increase.

In addition to conventional designs, contemporary techniques like as laser surface texturing have enabled the precise fabrication of micro-scale textures, allowing researchers to systematically investigate their impacts [13]. The results confirm that proper texturing enhances film thickness, stabilizes lubricant flow, and prolongs bearing lifespan. Nonetheless, a persistent limitation associated with texturing is the occurrence of cavitation, which may compromise the intended benefits.

Cavitation poses a significant issue in the functioning of lubricated thrust bearings, especially those featuring surface texturing. This phenomenon transpires when the local lubricant pressure diminishes beneath the vapor pressure, leading to the creation of vapor cavities or bubbles [14]. The bubbles may collapse violently when moved into regions of higher pressure, resulting in pressure fluctuations, noise, vibration, and possible surface damage. Cavitation substantially modifies the pressure distribution in the fluid layer of hydrodynamic thrust bearings and diminishes the effective LCC. Abass et al. [15] utilized computational fluid dynamics (CFD) – fluid-structure interaction (FSI) simulations to examine cavitation in journal bearing, revealing a reduction in maximum oil film pressure of roughly 17%. Comparable phenomena have been noted in thrust bearing, where closed-type patterns generate localized low-pressure regions that induce cavitation [16]. Such effects diminish the dependability and efficiency of bearings, compromising the advantages of texturing. While cavitation is typically harmful, certain studies indicate that under particular conditions, it may diminish friction by producing micro-lubrication effects at elevated eccentricity ratios [17]. Nonetheless, the overall effect is detrimental, as the instability and unpredictability of cavitation surpass any potential advantages. Consequently, cavitation control has emerged as a pivotal focus in thrust bearing design.

Mitigation strategies include optimizing pocket geometry, modifying texture distribution, and controlling lubricant properties. However, these solutions are not consistently sufficient, requiring the creation of innovative techniques to efficiently reduce cavitation while maintaining the tribological advantages of texturing. This challenge has led to an increased emphasis on slip engineering as an adjunct or alternative method. Slip engineering introduces the concept of partial slip at the lubricant-solid interface, which may be strategically utilized to regulate fluid flow and pressure distribution. In contrast to traditional surfaces that adhere to no-slip boundary conditions, slip surfaces provide enhanced lubricant mobility, thus diminishing shear resistance and altering pressure accumulation [18]. Slip can be improved via surface coatings, including hydrophobic or superhydrophobic films, or by engineering nanoscale structures that produce an apparent slip effect.

The advantages of slip surfaces in tribological systems are considerable. Initially, slip diminishes friction by lowering viscous drag. Furthermore, it can mitigate cavitation by modulating pressure gradients and averting sudden local pressure declines [19]. Third, when integrated with surface texturing, slip surfaces may augment load capacity beyond the constraints of texturing alone. Zhang [20] shown that the incorporation of boundary slippage at both the fixed inlet and the dynamic outlet regions of a step bearing could enhance the LCC by several hundred percent, concurrently diminishing friction. Zhang [21] subsequently expanded this concept to slanted pad thrust slider bearing, demonstrating that when slippage encompasses around 80% of the lubricated area, the load capacity increases by as much as 30% and the friction coefficient diminishes by over 40%. The results underscore that the position and magnitude of slip zones are essential design factors for enhancing hydrodynamic lubrication efficacy.

Nonetheless, slip engineering must be conducted with caution. Improper positioning of slip boundaries may lead to inadequate hydrodynamic pressure generation, undermining lubrication efficacy. When slip is assigned to regions chiefly accountable for load support, the decrease in viscous shear may result in reduced pressure rather of an increase. Thus, hybrid approaches that include slip and texturing at precisely chosen locations are considered the most efficacious.

Research in this field is still in its infancy, and comprehensive researches on slip-texture-cavitation relationships are limited. This requires comprehensive modeling techniques that include these factors to guide the logical design of thrust bearings. Due to the complex interactions among texturing, cavitation, and slip, experimental methods alone are insufficient to clarify their interconnected effects. CFD has thus become a crucial tool for the analysis of thrust bearings. CFD enables detailed simulation of lubricant flow, pressure distribution, cavitation phenomena, and slip boundary conditions in controlled virtual settings [12], [22]. The effectiveness of CFD lies in its ability to systematically adjust parameters like texture depth, slip distribution, and film thickness, allowing researchers to identify their effects without the costs and limitations of experimental setups. Additionally, advanced cavitation models and multiphase flow solvers have been integrated into CFD frameworks, enabling precise forecasts of vapor formation and collapse.

Many studies [4,15,22] have successfully employed CFD to predict the effects of texturing and cavitation on bearing performance, while more recent investigations [23,24] incorporate slip conditions into the models. These efforts produce substantial insights into the combined effects of different design components. Nonetheless, comprehensive CFD evaluations that simultaneously evaluate texturing, cavitation, and slip engineering in thrust bearings remain scarce. The prior description unequivocally demonstrates that thrust bearings are essential elements in various industrial applications, where LCC is a critical performance metric. Surface texturing significantly enhances lubrication effectiveness but may induce cavitation under unfavorable conditions. Cavitation negatively impacts bearing reliability and efficiency, requiring suitable management techniques. Slip engineering has tremendous promise to decrease cavitation and optimize pressure distribution; yet, its fusion with texturing remains underexplored. CFD provides a comprehensive approach to analyze these interrelated processes; nevertheless, extensive studies incorporating all three—texturing, cavitation, and slip—are few.

The novelty of this work lies in the integration of slip boundary conditions, surface texturing, and cavitation modeling within a single CFD framework for thrust bearings. Unlike previous studies that treated these mechanisms individually, this research systematically investigates their combined influence on hydrodynamic pressure distribution, cavitation behavior, and LCC under varying lubricant film thicknesses. Furthermore, the study identifies the optimal placement of slip zones on the stator surface that enhances load support while suppressing cavitation onset. These contributions provide new insights into the coupled effects of slip and texture engineering, establishing a foundation for advanced CFD-based optimization of thrust bearing performance.

2. METHODOLOGY

2.1. Governor equations

The hydrodynamic thrust bearing model requires the solution of fundamental conservation equations subject to appropriate boundary conditions. In this study, the governing equations consist of the continuity, momentum, and energy equations, which are expressed explicitly as follows [25]:

Continuity equation:

$$\frac{\partial u}{\partial x}+\frac{\partial v}{\partial y}+\frac{\partial w}{\partial z}=0 \tag{1}$$

Momentum equation:

$$\rho\left(u\frac{\partial u}{\partial x}+v\frac{\partial u}{\partial y}+w\frac{\partial u}{\partial z}\right)=-\frac{\partial p}{\partial x}+\mu\left(\frac{\partial^2 u}{\partial x^2}+\frac{\partial^2 u}{\partial y^2}+\frac{\partial^2 u}{\partial z^2}\right) \tag{2}$$

Energy equation:

$$\rho C_p\left(u\frac{\partial T}{\partial x}+v\frac{\partial T}{\partial y}+w\frac{\partial T}{\partial z}\right)=\lambda_f\left(\frac{\partial^2 T}{\partial x^2}+\frac{\partial^2 T}{\partial y^2}+\frac{\partial^2 T}{\partial z^2}\right)-\tau:\nabla V \tag{3}$$

where u, v, and w are the velocity components in the x, y, and z directions, respectively; V is the velocity vector (m/s); p is the static pressure (Pa); T is temperature (K); τ is the shear stress tensor; ρ is lubricant density (kg/m^3), μ is dynamic viscosity (Pa.s); C_p is specific heat (J/kg.K); and λ_f is thermal conductivity (W/m.K).

The Schnerr–Sauer model was employed for cavitation modeling. Equation (4) delineates the notion of vapor generation, with R denoting the rate of vapor generation, α signifying the vapor volume percentage, and ρ_v indicating the vapor density [26].

$$R=\frac{\partial}{\partial t}(\alpha\rho_v)+\frac{\partial}{\partial x_j}(\alpha\rho_v U_j) \tag{4}$$

This model is based on the Rayleigh–Plesset equation, which delineates the dynamics of vapor bubble formation and collapse in a liquid medium. Cavitation is seen as a mass transfer process between liquid and vapor phases, characterized by two source elements in the vapor transport equation that correspond to bubble development (evaporation) and collapse (condensation).

The condition for bubble rupture or collapse is determined by the local pressure field. When the local static pressure p surpasses the vapor pressure p_v. The vapor bubbles destabilize and implode, transferring mass from the vapor phase to the liquid phase [26]. The rate of mass transfer during condensation is represented by Equation (5).

$$\dot{m}_{cond}=\frac{3\alpha_v\rho l}{R_b}\sqrt{\frac{2}{3}\frac{p-p_v}{pl}} \tag{5}$$

where α_v denotes the vapor volume fraction, ρl is the liquid density, and R_b represents the bubble radius. The pressure difference (p-p_v) serves as the driving force for bubble collapse.

The rupture process physically entails the condensation of vapor cavities as the pressure rises above the vapor pressure. This collapse may produce localized pressure surges, micro-jets, and shock waves within the lubricant film, potentially leading to surface erosion or instability in the bearing's load-bearing layer. In hydrodynamic thrust bearings, vapor bubbles generally develop in low-pressure areas adjacent to the trailing edge of the pad and then collapse in regions of pressure recovery. The Schnerr–Sauer model accurately represents this dynamic cavitation activity inside the lubricant film.

This work includes slip boundary conditions and surface texturing effects. The interaction among cavitation, texturing, and slip strongly influences the pressure distribution and LCC of the bearing. The implementation of partial slip modifies the near-wall velocity gradient, potentially decreasing shear stress and altering local pressure recovery characteristics, particularly in cavitating areas. The existence of micro-textures, like dimples or grooves, facilitates localized pressure fluctuations and bubble nucleation, hence affecting the initiation and collapse of cavitation. The integration of these three elements—texture, cavitation, and slip—facilitates a more precise forecast of lubrication efficacy and provides critical understanding of how micro-scale surface engineering can be employed to regulate cavitation dynamics and improve the operational efficiency of hydrodynamic thrust bearings.

The interfacial limiting shear strength model, also known as the critical shear stress model, as proposed by Zhang [27], is utilized for modeling the boundary slip effect. In this model, slip occurs exclusively when the wall shear stress surpasses a critical threshold, τ_{oc}, which denotes the interfacial shear strength between the lubricant and the solid surface. Upon reaching this threshold, slip occurs with a consistent characteristic length b' that remains unchanged during the process. The governing relationship is represented by the Equation (6).

$$\tau_c = \tau_{oc} \frac{u_s}{b'} \eta \qquad (6)$$

where τ_c, is the total interfacial shear stress, u_s is the slip velocity, η is the dynamic viscosity of the lubricant, and b' denotes the equivalent slip length. This model delineates the transition from the no-slip condition to the slip condition when the interfacial shear stress surpasses its critical threshold, in accordance with the framework outlined in Zhang's review on hydrodynamic lubrication featuring interfacial slippage [27].

Based on the findings of the present study, the LCC is determined by integrating the pressure throughout the surface area of the rotor. When these equations were solved with Ansys Fluent, a numerical solution was generated as a result.

2.2. CFD Modeling

The geometry modeled represents a hydrodynamic thrust bearing featuring circumferential pocket surface texturing and eight stator pads. The circumferential pocket geometry consists of four surrounding channels that direct fluid flow in accordance with the rotation of the stator. The pocket or surface texture geometry pertains to the design proposed in [28], while the lubricant film thickness and groove geometry conform to the standards utilized by [29]. Further modifications were implemented to the geometry utilized in this work to accommodate a range of pocket depths. The geometry presented here is based on findings from prior research [12].

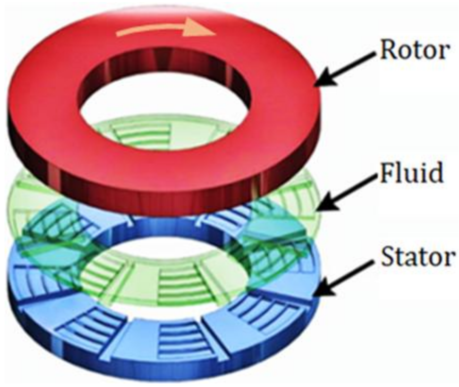

(a)

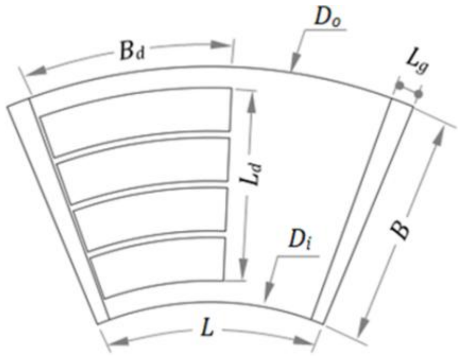

(b)

Fig. 1. The circumferential hydrodynamic thrust bearing, (a) rotor, fluid, and textured stator and (b) the fluid domain and its nomenclature.

Figure 1 presents the geometric configuration and dimensions used in this study, while Table 1 outlines these parameters in detail, including the minimum film thickness (H_{min}), which represents the lubricated gap between the stator and rotor.

Table 1. Dimensions of the circumferential pocket of thrust bearing.

Parameters	Value	Unit
Length of stator (L)	45	deg
Width of stator (B)	20	mm
Length of groove (L_g)	2.46	deg
Depth of groove (H_g)	4	mm
Outside diameter (D_o)	90	mm
Inside diameter (D_i)	50	mm
Length of pocket (B_d)	56.20%L	deg
Width of pocket (L_d)	84.70%B	mm
Depth of pocket(H_d)	30	µm
Minimum film thickness (H_{min})	15, 20, 25, 30, 40, 50, 80	µm

Boundary conditions were applied to all of the key geometrical surfaces, such as the inlet and outlet surfaces, the faces of the rotor and stator, two periodic surfaces, and a no-slip condition with a rotational speed of 6000 rpm. The Schnerr–Sauer model was utilized for the purpose of modeling cavitation. In Figure 2, the boundary conditions are depicted, and Table 2 contains the parameters. The outlet (Fluid Outer Surface) is defined as an opening boundary with static relative pressure = 0 bar and temperature = 20 °C, following the validation setup of Chalkiopoulos et al. [29]. These values are applied as environmental reference boundary conditions in the CFD model; although the energy equation is included in the governing system, detailed thermal results are not reported in this study as the focus is on hydrodynamic pressure and LCC.

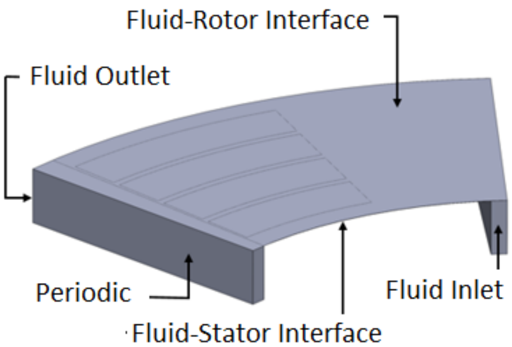

Fig. 2. The boundary condition of the CFD.

The lubricant utilized in the simulations was ISO VG 46 oil, which is defined by laminar flow and a no-slip condition at 6000 rpm. The lubricant parameters were extracted from the data presented in reference [9], and the cavitation pressure settings were sourced from the research conducted by Koutsoumpas et al. [30]. Table 3 presents the lubricant parameters utilized in the simulation.

Table 2. Boundary condition.

Conditions	Remarks
Periodic	Rotational
Inlet	Relative static pressure: 1 bar
	Temperature: 40 °C
Outlet	Relative static pressure: 0 bar
	Temperature: 20 °C
Rotational speed	6000 rpm

Meshing was performed using Ansys ICEM CFD. The structured mesh was developed by dividing the geometry into multiple blocks, which aids in grid alignment and improves mesh quality. The Pre-Mesh quality tool was utilized for mesh validation, evaluating the determinant of each mesh element to ensure compliance with established quality criteria. A minimal determinant value exceeding 0.3 is considered acceptable for accurate results [31]. The completed mesh for the geometry consisted of approximately 250,000 elements, as depicted in Figure 3.

Table 3. Lubricant parameters utilized in the simulation.

Parameters	Value	Unit
Density (ρ)	870	kg/m^3
Specific heat capacity (C_p)	2100	J/kg.K
Thermal conductivity (λ_f)	0.13	W/m.K
Dynamic viscosity at 40°C (μ_{40})	0.0416	Pa.s
Dynamic viscosity at 80°C (μ_{80})	0.0105	Pa.s
Density of gas (ρ_g)	1.185	kg/m^3
Thermal conductivity of gas (λ_{fg})	0.0261	W/m.K
Specific heat capacity of gas (c_{pf})	1004.4	J/kg.K
Dynamic viscosity of gas (μ_g)	0.00021	N·s/m^2
Cavitation pressure (P_c)	50	kPa

Figure 3 illustrates the mesh configuration for a model with a film thickness of 15 μm. The film region consists of three layers, while the pocket depth of 30 μm contains twelve layers, leading to a cumulative total of fifteen layers within the combined depth. The quantity of pocket layers varies based on the thickness of the lubricant film, while the depth of the pockets remains constant. The minimal film thickness (H_{min}) of 15 to 30 μm is composed of 3 layers, while the thickness of 40 to 80 μm is made up of 4 layers. The cumulative count of layers, specifically H_d and H_{min}, across all variations of the minimum film thickness is 15 layers. The meshing procedure involves the utilization of around 250,000 hexahedral elements.

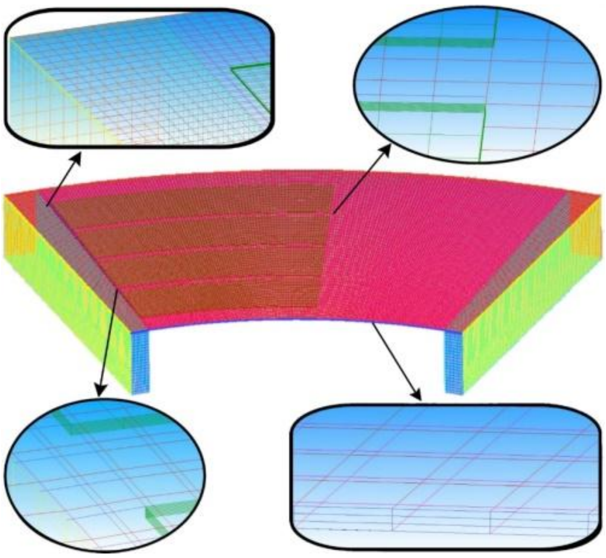

Fig. 3. Meshing in fluid domain.

The simulation is conducted using a laminar model, with the Energy option enabled. The fluid's viscosity parameters are configured using the Piecewise-Linear model, with the lubricant's specifications being inputted into the Ansys Fluent software. This software was selected because to its inclusion of the slip setting menu. Ansys Fluent is employed in this CFD modeling. The convergence criterion for this simulation, as determined by the root mean square residual value, is 1E-5. The solution method is specified as SIMPLEC and the pressure is chosen to be Second Order. Both the Momentum and Energy schemes are configured to use Second Order Upwind. The work utilizes a 3.20 GHz central processing unit (CPU) of 16 CPUs. The RAM has a capacity of 32 gigabytes. Each simulation necessitates an approximate time 30 min.

Figure 4 demonstrates the slip locations identified in this study. Slip conditions were implemented in four configurations: (a) no-slip [NS], (b) slip-before-pocket [SBP], (c) slip-on- pocket [SOP], and (d) combined-slip, both before and on pocket [SBPP]. No-slip pertains to a stator operating under conditions of absence of slip, while slip-before-pocket indicates the application of slip boundary conditions prior to the placement of the pocket. The slip-on-pocket denotes the implementation of slip boundary conditions at the location of the pocket or its texture. The slip-before-pocket and on pocket, or combined-slip, pertains to the distribution of slip locations in the area preceding and within the pocket region. The relatively small slip area was inspired by the geometry proposed by Chalkiopoulos et al. [29] and is justified by the ratio between the textured and smooth regions—commonly referred to as a heterogeneous surface. This proportion aims to achieve an optimal balance between slip-induced pressure enhancement and surface stability.

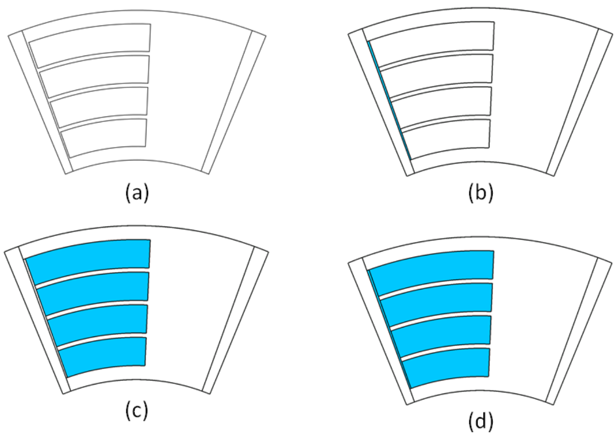

Fig. 4. The slip locations are marked in blue, (a) no-slip [NS], (b) slip-before-pocket [SBP], (c) slip-on-pocket [SOP], and (d) combined-slip, before and on pocket [SBPP].

Prior to simulations, model validation was performed. The verified case utilized a multi-texture thrust bearing configuration with a lubrication layer of 40 μm, a multitexture pocket depth of 20 μm, a rotational speed of 6000 rpm, ISO VG 46 oil, and laminar flow conditions. The comparison of maximum pressure in this study with that of [29] showed a variation of only 0.55%, indicating strong agreement and supporting the validity of the current simulation methodology. Figure 5(a) illustrates that the pressure profile from the present study is in close agreement with previous simulation results. The data used for plotting pressure profiles were obtained along the midline of an individual bearing pad. Reference [29] utilized radial plot R34; however, this study employed R36, which is associated with the midpoint of the pocket and the maximum pressure zone in a circumferential pocket thrust bearing with H_d = 30 μm. The rationale for this decision is supported by the pressure distribution depicted in Figure 5(b).

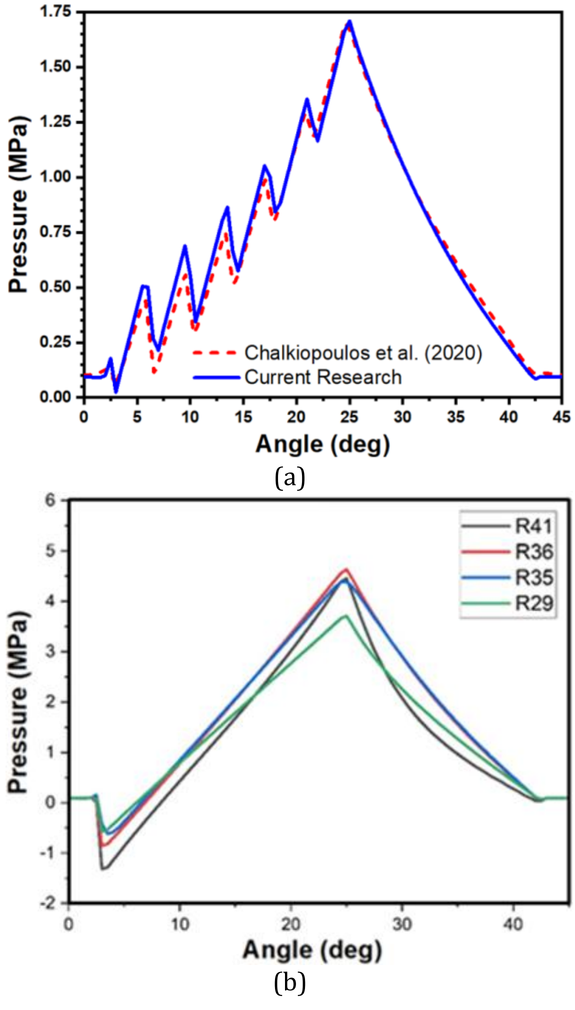

Fig. 5. (a) Validation of the current research with the previous investigation [29] and (b) the pressure profile of circumferential pocket at various radial positions, with R36 selected in this study.

Mesh independence tests verified that the simulation results were not significantly affected by the number of mesh elements. Figure 6 depicts the test outcomes with nearly 250,000 elements, where the maximum pressure reached was 1.709 MPa, yielding only a 1% variance. This verifies that the employed mesh size, which is below the 300,000 elements indicated in [29], reduces computing costs while preserving accuracy. This study focuses on the hydrodynamic pressure generated as the basis for calculating the LCC. It excludes any discourse about temperature.

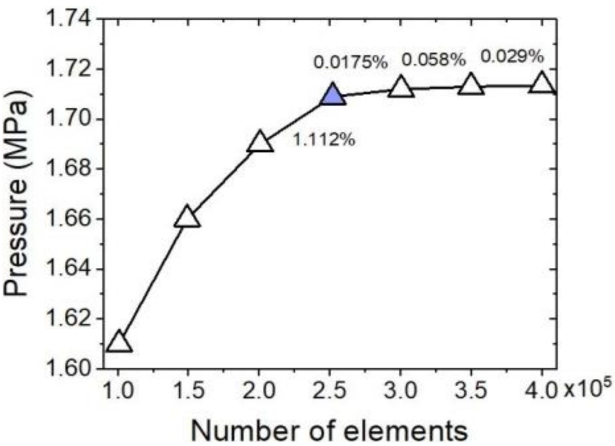

Fig. 6. Grid independence test.

3. RESULTS AND DISCUSSION

This study performed a simulation analysis on a circumferential pocket-type hydrodynamic thrust bearing with a pocket depth of 30 μm. Variations in lubricant film thickness measured 15 to 80 μm. The slip conditions implemented on the stator surface were categorized into four distinct types: no-slip, slip-before-pocket, slip-on-pocket, and a combination of slip-before-pocket and slip-on-pocket. The simulations incorporated cavitation conditions, employing laminar flow at a rotational speed of 6000 rpm. The discussion will encompass both cavitation analysis and modeling in the absence of cavitation conditions. This analysis seeks to clarify the distinctions between the two models.

3.1. Effect of slip formations on the pressure distribution

Figure 7 demonstrates that the maximum pressure across all lubricant film thicknesses was consistently highest in the slip-before-pocket configuration, while the lowest pressure values were recorded in the slip-on-pocket configuration. The maximum pressure values under combined slip conditions for film thicknesses of 15 to 50 μm were lower than those recorded in the no-slip scenario.

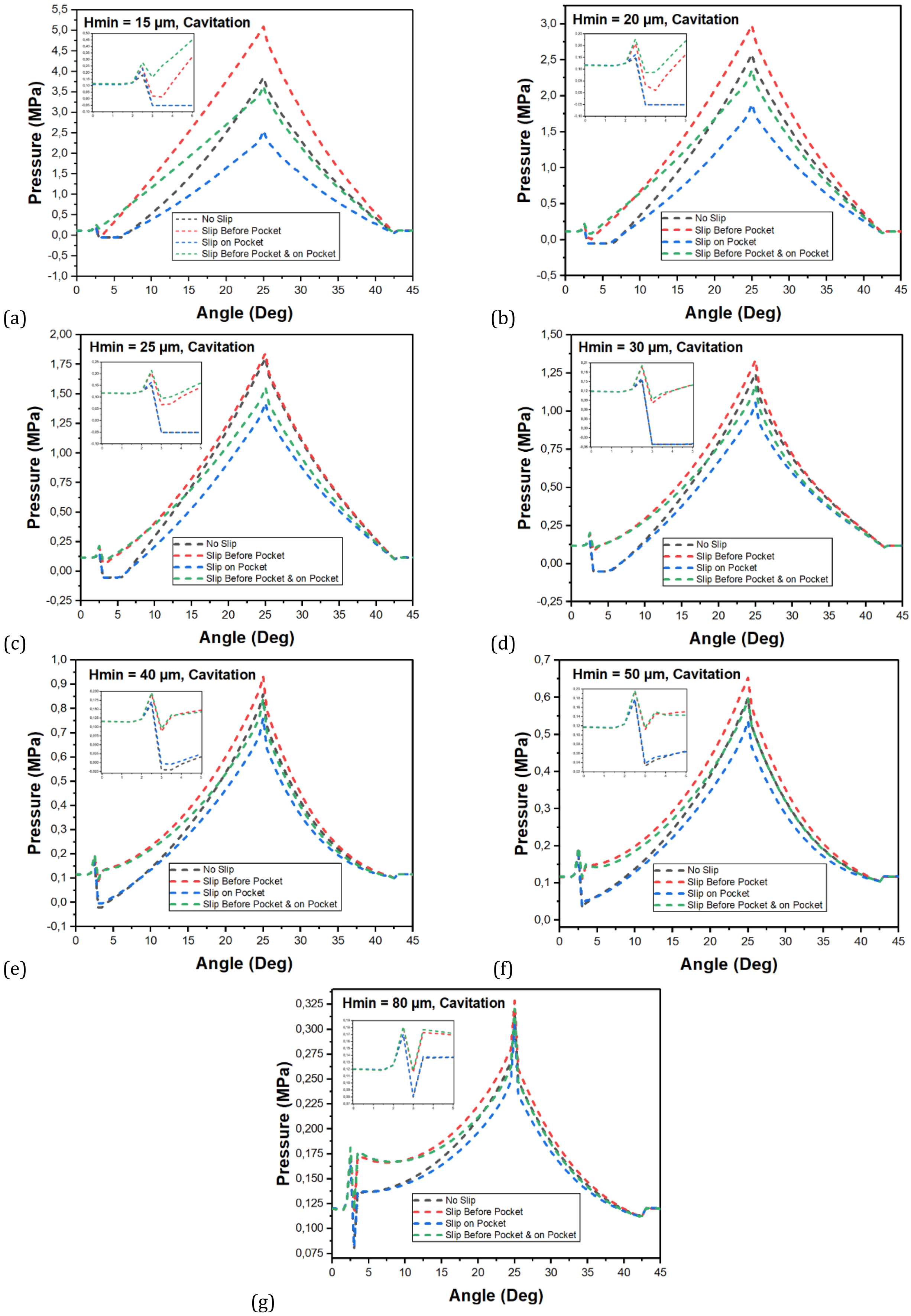

Fig. 7. The hydrodynamic pressure profiles of the varied slip formations at the different minimum film thicknesses in cavitation condition.

At a film thickness of 80 µm, the maximum pressure under combined-slip conditions exceeded that of the no-slip configuration. The results indicate that applying slip on the stator surface enhances pressure performance in hydrodynamic thrust bearing. The application of slip before the pocket led to a significant increase in pressure compared to the no-slip condition. The improper placement of slip, specifically the combined-slip condition of 15 to 50 µm and slip directly on the pocket, negatively affected pressure performance, resulting in lower maximum pressures relative to the no-slip configuration. The cavitation modeling indicates that if the lubricant pressure falls below the established cavitation pressure of 0.05 MPa, the pressure will remain constant at that level until an increase occurs. This event occurs at the leading edge, the site of the cavitation phenomenon. The stable pressure observed in the cavitation area in this investigation aligns with findings from previous studies [32-34].

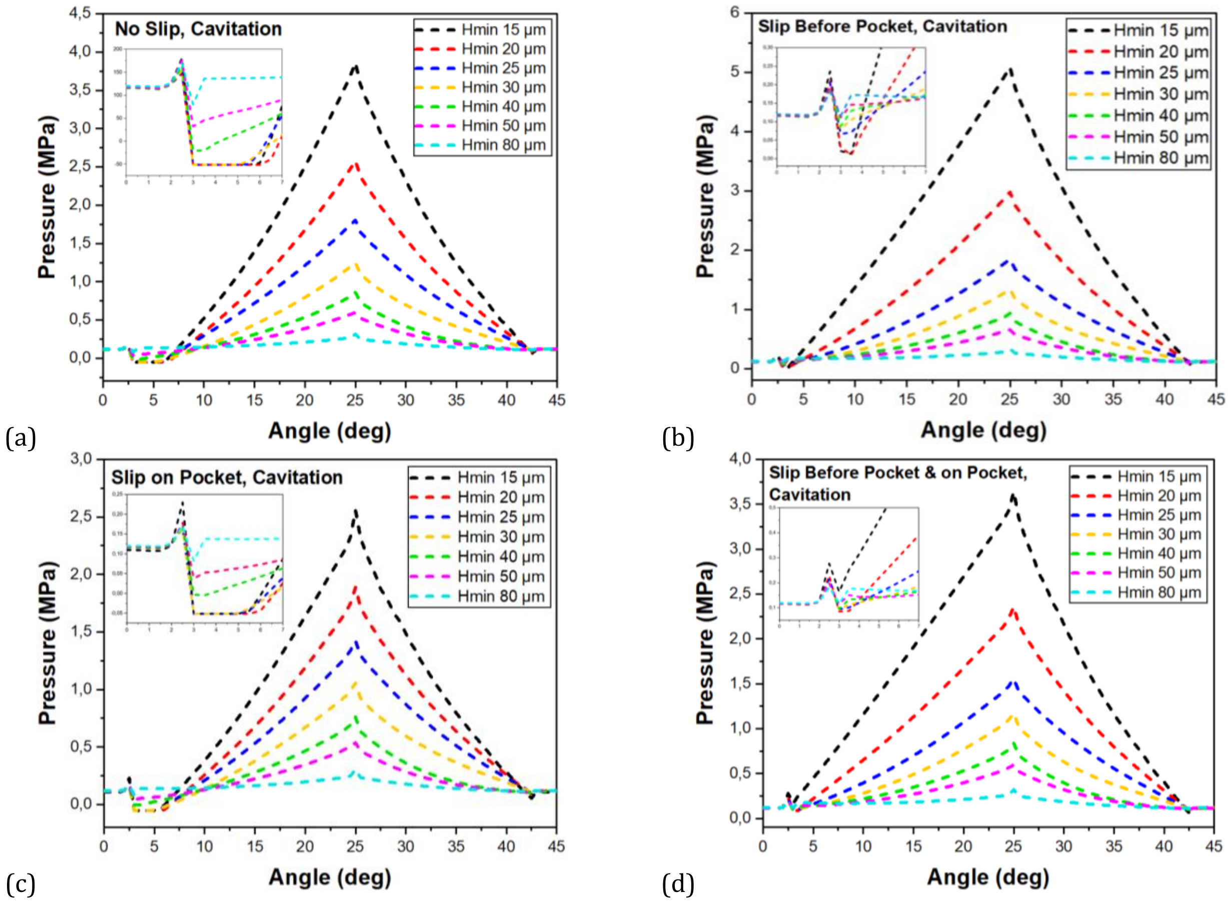

Fig. 8. Comparing the pressure distribution under four different slip situations to the differences in the minimum film thickness.

Figure 8 illustrates that for each slip scenario, the maximum pressure occurred at a lubricant film thickness of 15 µm, whereas the minimum pressure was consistently observed at 80 µm. This supports the notion that thinner lubricant films result in higher pressure, aligning with the findings of [8], which demonstrate that bearing load is notably affected by the separation between two solid surfaces. As film thickness increases, the LCC decreases in a nonlinear manner. The maximum pressure recorded was 5.09 MPa at a film thickness of 15 µm under the slip-before-pocket condition, whereas the minimum pressure observed was 0.305 MPa with an 80 µm film thickness in the no-slip condition. The formation of slip at the location prior to the pocket enhances fluid flow, accelerating the movement of lubricant from this area into the pocket. The lubricant pressure increases upon the fluid's arrival at the pocket due to the residual slip effect originating from the upstream region. However, as the flow continues, the momentum gained in the slip zone reduces the viscous shear contribution to pressure generation, causing a small pressure drop below the inlet level.

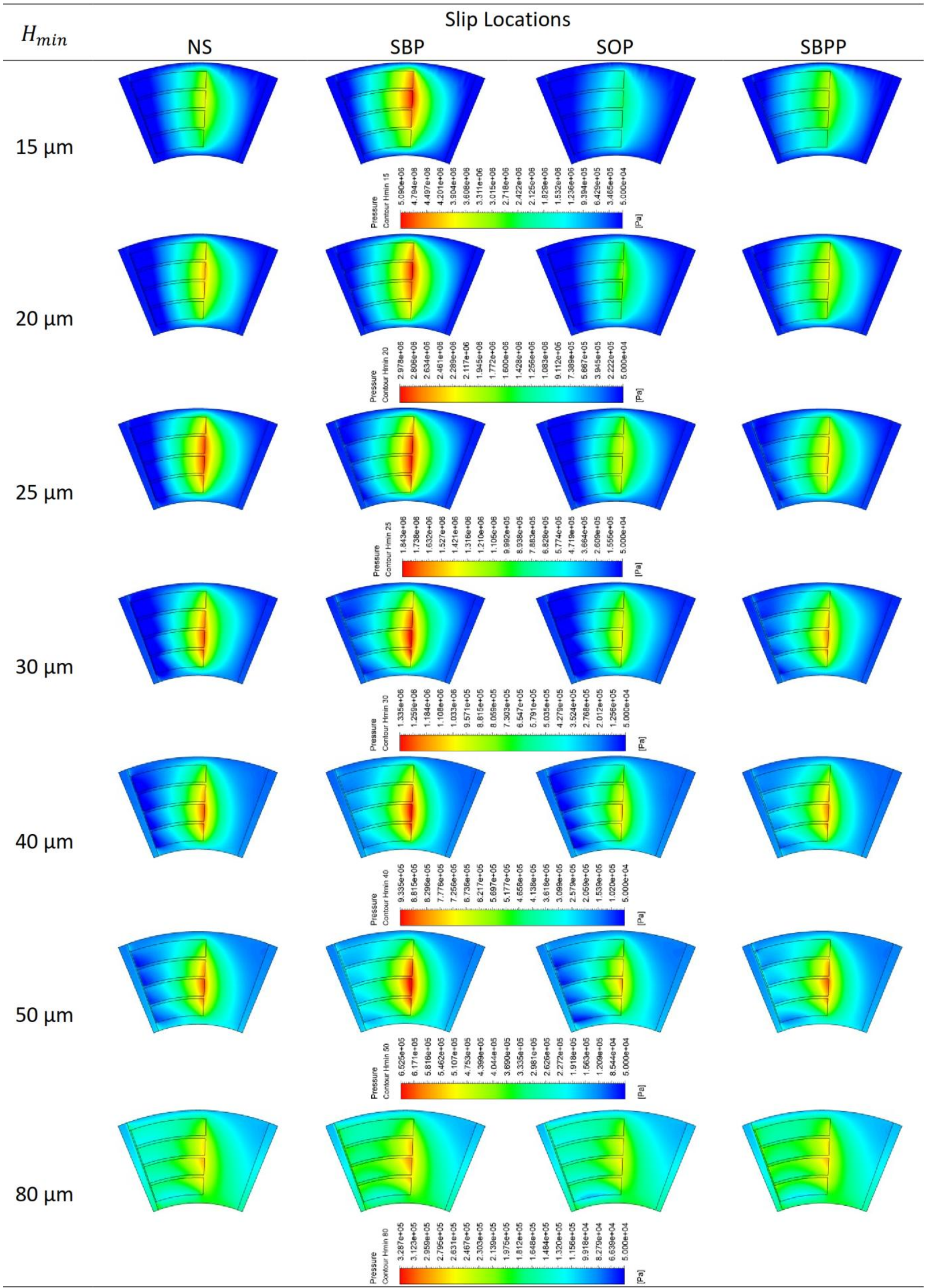

Fig. 9. Contour plots of pressure distribution in circumferential thrust bearing under cavitation conditions, evaluated at various minimum film thicknesses for four slip configurations: no-slip (NS), slip-before-pocket (SBP), slip-on-pocket (SOP), and combined-slip (SBPP: before and on pocket).

Figure 9 presents that the minimum pressure for both no-slip and slip conditions at a film thickness of 15 to 30 μm reached the cavitation threshold of 0.05 MPa. This indicates a significant likelihood of cavitation formation in specific regions. The implementation of slip-before-pocket and combined-slip arrangements significantly improved the minimum pressure, suggesting enhanced lubrication conditions and a reduced risk of cavitation. The application of slip is observed to reduce the cavitation region, as shown in Figure 9(b). This finding aligns with the results documented in [32,33]. A reduced cavitation zone positively influences the enhancement of hydrodynamic pressure produced by the lubricant. The placement of slip regions significantly influences the resulting pressure. Strategically positioned slips can enhance pressure accumulation and reduce cavitation effects. These findings are consistent with [35], which demonstrated that the application of slip can reduce areas prone to cavitation, thereby mitigating its occurrence.

Figure 9 illustrates the pressure distribution contours of circumferential thrust bearing under cavitation conditions, indicating variations in minimum film thickness ranging from 15 to 80 μm across four slip configurations: no-slip (NS), slip-before-pocket (SBP), slip-on-pocket (SOP), and combined-slip (SBPP – before and on pocket). The SBP configuration consistently produces higher hydrodynamic pressure compared to the other three slip conditions across all variations of minimum film thickness (H_{min}). The maximum pressure is recorded at H_{min} 15 μm (approximately 5 MPa), whereas the minimum is noted at H_{min} 80 μm (approximately 0.3 MPa). The observation reveals that pressure concentration is predominantly localized at the end region of the pocket situated in the middle part of the bearing. It subsequently dissipates, decreasing towards the periphery of the pocket and the adjacent no pocket region. At a minimum film thickness of 15 μm, the slip state preceding the pocket exhibits a dark blue color, signifying the occurrence of cavitation. This observation indicates that the pressure at the specified location, including the leading edge, is below 0.05 MPa. This work examines a variation in pressure concentration at the center of the bearing (see SBP in H_{min} 15) in contrast to the findings of Syafaat et al. [12], who indicated that with a pocket depth of H_d 20 μm, slip engineering successfully shifted the center of pressure outward from the bearing. This study's findings demonstrate that the H_d 30 μm pocket depth does not displace the pressure concentration outward from the bearing, which contrasts with the results of prior research. The bearing pressure exhibits greater stability at a pocket depth of 30 μm in comparison to a depth of 20 μm. The research indicated that a rise in minimum film thickness is associated with a decreased probability of cavitation events.

The incorporation of slip in the area preceding the pocket facilitates fluid flow, enabling the fluid to exit the slip region and enter the pocket with more ease. Slip designed to enable the lubricant's release from this region and its subsequent ingress into the pocket. As the fluid enters the pocket, the residual slip effect from the upstream region elevates the lubricant pressure. The dynamics of lubricant velocity contours were previously documented by Syafaat et al. [12].

3.2. Effect of Slip Formations on the LCC

Figure 10 shows the LCC performance obtained from CFD simulations of the circumferential pocket hydrodynamic thrust bearing under cavitating flow conditions. The investigation employed a fixed pocket depth (H_d) of 30 μm and variations in lubricating film thickness ranging from 15 to 80 μm. The slip configurations included NS, SBP, SOP, and SBPP. The findings demonstrate that for all slide configurations, the peak LCC value consistently appeared at H_{min} 15 μm, whilst the lowest LCC was noted at H_{min} 80 μm.

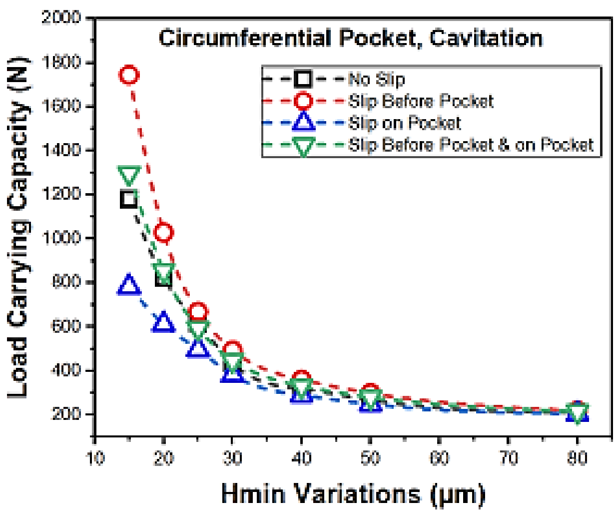

Fig. 10. Comparison of the LCC in cavitation modeling under varied slip locations and minimum film thicknesses.

The slip before pocket arrangement exhibited superior LCC performance across all film thicknesses, while the SOP structure yielded the lowest LCC values in every case. The maximum LCC recorded across all combinations of slip and film thickness was 1744.61 N, seen at a film thickness of 15 μm with slip before the pocket. The minimum LCC was 204.52 N at a film thickness of 80 μm under SOP formation.

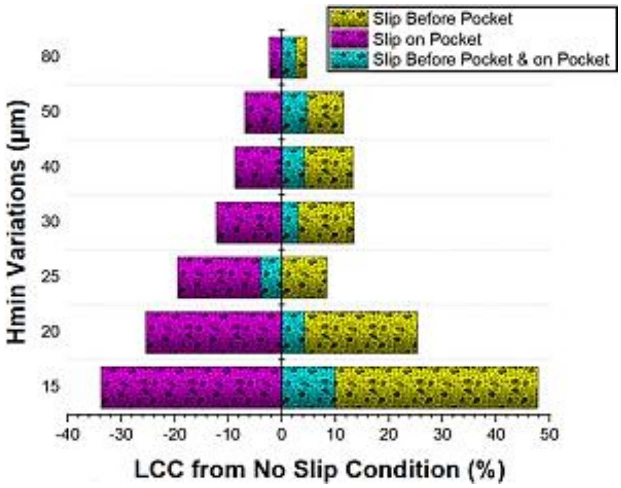

Fig. 11. Change in the LCC from no-slip condition to slip conditions in cavitation modeling.

Figure 11 illustrates the percentage change in LCC from the no-slip condition to the three slip setting conditions examined in this study. Among the three slip applications (SBP, SOP, SBPP), the most notable improvement compared to no slip was found with slip-before-pocket at H_{min} 15 μm, yielding a 47.76% increase. The most notable decline was observed in the slip-on-pocket at the same film thickness, with a reduction of -33.79%. The percentage increase in LCC for slip before pocket compared to no-slip generally decreased with greater film thickness, except at H_{min} 25 μm, which was slightly lower than the result at 30 μm. The slip-on-pocket demonstrated a gradual increase in LCC % change with increasing film thickness, yet consistently remained below the no-slip baseline. The data underscore the importance of slip location. The slip-before-pocket method significantly enhances load support, particularly with thinner lubricant films, while the slip-on-pocket approach tends to reduce LCC especially in thin-film conditions.

Figure 11 is derived from the data presented in Figure 10, where the LCC values for each slip configuration are plotted. While Figure 10 focuses on the trend of LCC variation as a function of minimum film thickness, Figure 11 expresses the percentage change in LCC relative to the no-slip condition. A negative LCC value represents a reduction in LCC compared with the no-slip condition, rather than an actual loss of lubrication. This means that slip engineering does not always yield beneficial effects. A positive LCC percentage indicates performance improvement, whereas a negative value signifies performance deterioration relative to the baseline case. Nevertheless, hydrodynamic lubrication is still maintained under all simulated conditions—the entire load is supported by the lubricant film, ensuring that no direct contact occurs between the rotor and stator surfaces. Therefore, the negative LCC value observed for the SBPP configuration at a minimum film thickness of 25 μm represents a local decrease compared to the baseline, not an actual loss of load support. The negative % change in LCC at H_{min} 25 μm occurs because this thickness represents a transition zone between thin-film and thicker-film regimes. In this range, the accelerated flow caused by slip before or on the pocket reduces the local shear and pressure recovery, leading to a relative decrease in LCC under cavitation.

3.3. Effect of no cavitation modeling on the pressure distribution

Figure 12 indicates that, under the no-slip condition with a film thickness of 15 μm, the maximum pressure in the no cavitation simulation reached 4.63 MPa. Under cavitation, the same condition resulted in 3.86 MPa, indicating a decrease of 16.63%. The maximum pressure in the slip-before-pocket arrangement under no cavitation conditions was 5.60 MPa, while with cavitation it decreased to 5.09 MPa, indicating a reduction of 9.10%. The maximum pressure under the slip-on-pocket configuration decreased from 2.91 MPa in the absence of cavitation to 2.56 MPa with cavitation, reflecting a reduction of 12.02%. In the combined slip configuration, the maximum pressure decreased from 4.13 MPa under non-cavitating conditions to 3.64 MPa with cavitation, indicating a reduction of 11.86%. The findings validate that cavitation adversely impacts the maximum pressure in thrust bearing, aligning with the observations noted by Chen et al. [14]. This outcome, however, contrasts with earlier findings, such as those by Muchammad et al. [36], which indicated that simulations including cavitation produced higher pressure levels than those without cavitation.

3.4. Effect of No Cavitation Modeling on the LCC

The comparisons of LCC between simulations with and without cavitation closely mirrored the trends observed in maximum pressure. Under the no-slip condition, the LCC attained a peak value of 1493.62 N for H_{min} 15 µm in the absence of cavitation, which decreased to 1180.64 N when cavitation was present, indicating a reduction of 20.95%. The LCC decreased from 2049.45 N (no cavitation) to 1744.61 N (cavitation), reflecting a reduction of 14.87%. The slip-on-pocket configuration exhibited a decrease in LCC from 941.61 N under no cavitation conditions to 781.59 N with cavitation, indicating a reduction of 16.99%.

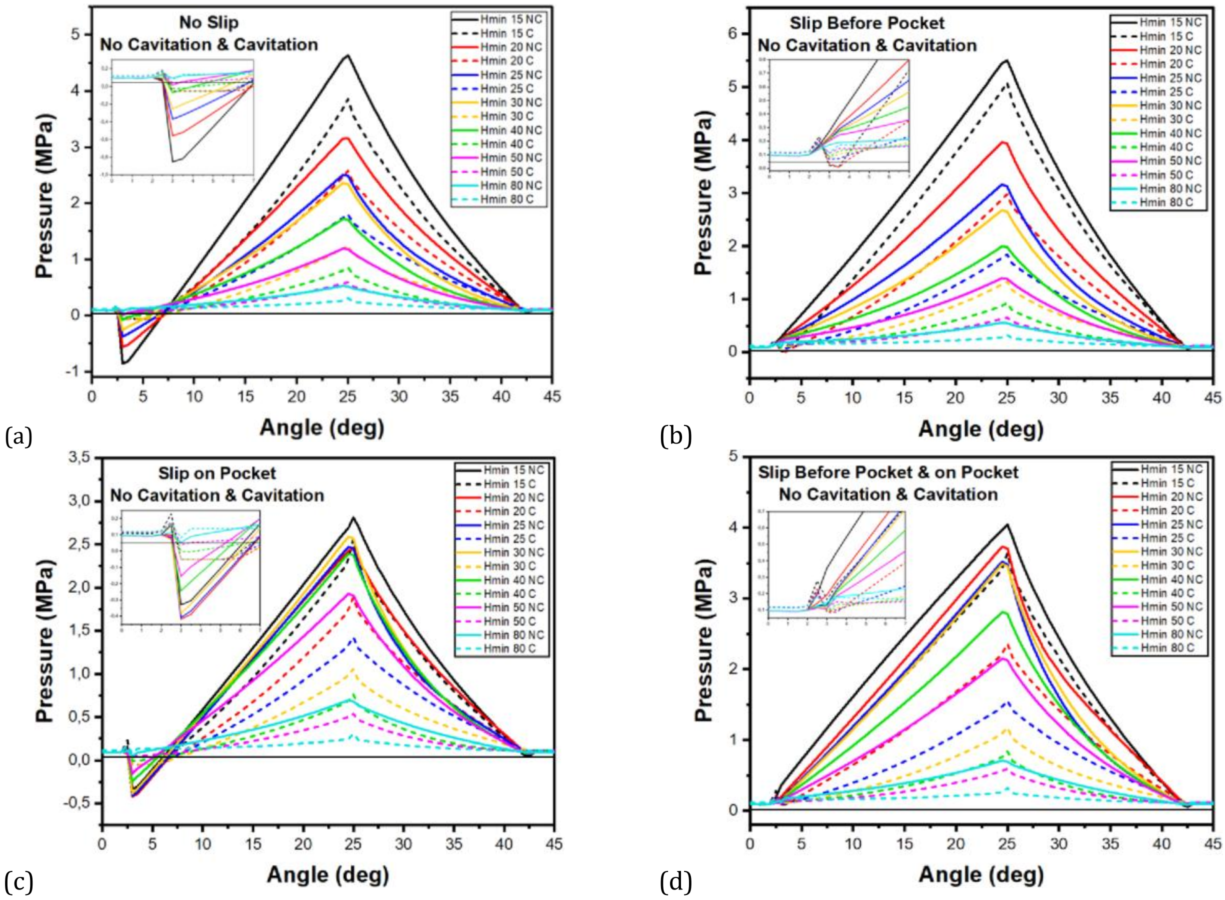

Fig. 12. Comparison of the pressure distribution under both no cavitation (NC) and cavitation (C) modeling in variations of H_{min} for conditions: (a) no-slip, (b) slip-before-pocket, (c) slip-on-pocket, and (d) slip-before-pocket and on pocket. The horizontal line represents the cavitation pressure of 0.05 MPa.

The cavitation LCC value was notably lower than the no cavitation values for H_{min} values between 20 and 40 µm. In the combined-slip configuration, the LCC decreased from 1562.15 N (no cavitation) to 1297.91 N (cavitation), indicating a reduction of 16.91%. Additionally, this value was lower than the LCC at H_{min} 20 µm (1354.46 N) under no cavitation conditions.

Figure 13 presents a comparison of the LCC for circumferential thrust bearing with a pocket depth of 30 µm under both cavitation and non-cavitation conditions across various minimum film thicknesses. The results demonstrate that LCC consistently decreases with increasing film thickness across all configurations, supporting hydrodynamic lubrication theory—thinner lubricant films promote greater pressure accumulation and support larger loads. Cavitation consistently reduces LCC, as evidenced by the lower values of C relative to their NC counterparts. The effect is most significant for diminished film thicknesses, notably H_{min} 15 µm. Among several slip designs, the slip preceding the pocket configuration in conditions devoid of cavitation exhibits the highest LCC, reaching 2049.45 N at H_{min} 15 µm. In contrast, the slip-on-pocket condition during cavitation yields the least effective performance, particularly at increased film thicknesses, where LCC diminishes to roughly 200–300 N. The results demonstrate that inhibiting cavitation and properly placing slip—especially before to the pocket—can significantly enhance bearing performance, while slip on the pocket surface may be detrimental in cavitating flow conditions.

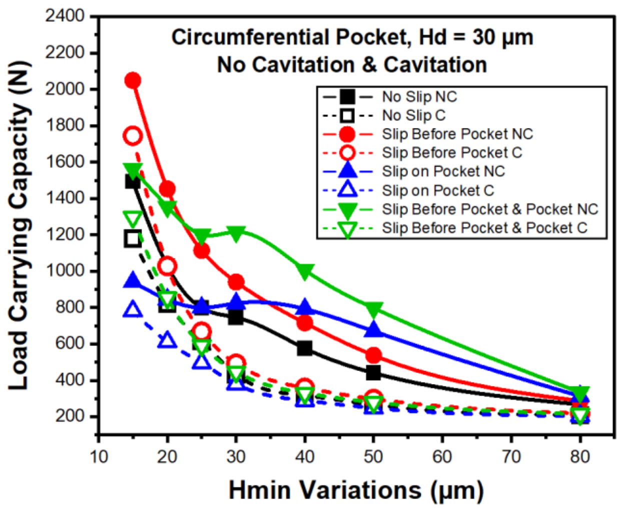

Fig. 13. The comparison of LCC both no cavitation (NC) and cavitation (C) modeling under varied slip locations and minimum film thicknesses.

Figure 14 displays the LCC comparison between the study and previous research [12], particularly for changes in pocket depth. Both research findings demonstrate a decrease in LCC associated with an increase in the thickness of the lubrication layer between the stator and rotor.

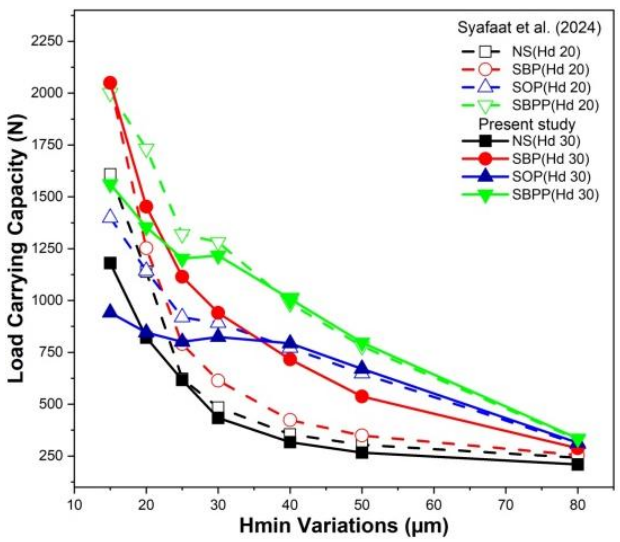

Fig. 14. Comparison of LCC results from the present study and prior research [12] conducted under cavitation flow condition.

This result is consistent with the current literature [1]. The second conclusion derived from the study's data is that an increase in pocket depth is associated with a reduction in LCC. Both research points are logically justified: to achieve a significant LCC, the minimal distance between the stator and rotor (H_{min} or H_d) is crucial, enabling the fluid to function as a barrier for transmitting force from the solid surface (rotor) to the fluid, which then transfers it to the adjacent solid surface (stator).

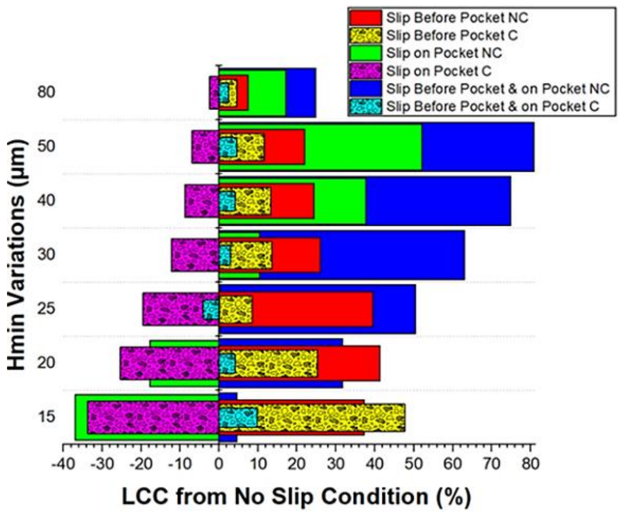

Fig. 15. Change in the LCC from no-slip condition to slip conditions under both no cavitation (NC) and cavitation (C) modeling.

Figure 15 depicts the percentage change in LCC compared to the no-slip baseline in both cavitation and non-cavitation scenarios. The most notable improvement was observed with the combined-slip configuration at a lubricant thickness of 50 μm under conditions devoid of cavitation, leading to an increase of 80.85%. The most notable reduction occurred in the slip-on-pocket configuration with a film thickness of 15 μm under the no cavitation condition, registering at -36.96%. In both cavitation and no cavitation scenarios, the percentage improvement in slip prior to pocket formation decreased as film thickness increased. In contrast, under no cavitation conditions, both the slip-on-pocket and combined-slip scenarios demonstrated increasing percentage gains up to a film thickness of 50 μm, followed by significant reductions at 80 μm. In the context of cavitation, all slip-on-pocket configurations demonstrated reductions in LCC compared to the no-slip scenario, with losses diminishing as film thickness increased. The maximum LCC gain observed under cavitation was 47.76%, achieved with slip-before-pocket at a film thickness of 15 μm. The most notable reduction was -33.79% for the slip-on-pocket at the same thickness. The data further substantiate that cavitation negatively affects LCC performance; supporting the claim in [14] that cavitation reduces the efficiency of hydrodynamic thrust bearing.

Figure 15 is based on the data shown in Figure 14, illustrating the LCC values for each slip arrangement. Figure 14 illustrates the trend of LCC variation as a function of minimum film thickness, whereas Figure 15 shows the percentage change in LCC in relation to the no-slip condition. A negative LCC number indicates a decrease in LCC relative to the no-slip condition, rather than a genuine loss of lubrication. This indicates that slip engineering does not consistently produce advantageous outcomes. A positive LCC percentage denotes performance enhancement, whereas a negative figure shows performance decline in comparison to the baseline scenario. Nonetheless, hydrodynamic lubrication is preserved under all simulated situations, with the lubricant film entirely supporting the load, so preventing direct contact between the rotor and stator surfaces.

Interestingly, at H_{min} 25 μm in the cavitation scenario, both the slip-before-pocket and slip-on-pocket designs resulted in a negative percentage change in LCC relative to the no-slip baseline (Figure 15). This behavior can be explained by analyzing the transition from an optimally thin (15-20 μm) to a thicker (30 μm and above) film regime. At this intermediate film thickness, the advantages of slip are counterbalanced by the modified hydrodynamic pressure accumulation and heightened cavitation risk: the pre-pocket slip hastens lubricant egress excessively, leading to a reduction in sustaining shear stress and a decline in pocket pressure recovery, while the pocket-slip condition fosters locally increased cavitation inception due to altered near-wall gradients. Prior research by Syafaat et al. [12] on pocket geometries with slip similarly shown that deviations from the optimal film-thickness range may result in performance deterioration due to texture or slippage. Consequently, the negative value at 25 μm underscores the necessity of concurrently adjusting film thickness, texture/slip zone dimensions, and positioning to stay within the advantageous range.

3.5. Comparison with the Zhang model

The impact of slip placement identified in this study aligns closely with the processes suggested by Zhang [20] and Zhang [21]. Zhang [20] analytically established that the incorporation of boundary slippage at the stationary inlet and dynamic outlet of a step bearing elevates hydrodynamic pressure by augmenting fluid entrainment and alleviating detrimental shear near the film peripheries. The slip-before-pocket arrangement in the current simulation generated the maximum pressure across all minimum film thicknesses, demonstrating that inlet-side slip significantly enhances Couette-driven flow and facilitates pressure accumulation in the pocket region. Zhang [21] demonstrated that a tilted-pad thrust bearing with regulated slip zones attained a LCC increase of up to 30% and a friction reduction above 40% when the slip region covered approximately 80% of the pad surface. Our findings align with this trend: excessive or misaligned slip (e.g., slipping directly on the pocket) undermines local shear support and decreases pressure, corroborating Zhang's assertion that poor slip positioning can diminish hydrodynamic pressure rather than augment it.

Zhang [27] asserted that interfacial slippage can enhance bearing performance only if the slip zone is meticulously managed to avert film disintegration. He also observed that slippage alters pressure gradients, therefore influencing the onset of cavitation. The current findings—where slip-before-pocket diminished the cavitation region but slip on the pocket exacerbated it—validate this theoretical understanding. Consistent with Zhang [27], the enhanced minimum pressure and reduced cavitation zone found herein validate that appropriately positioned slip mitigates cavitation by refining the pressure gradient at the leading edge. This substantiates the idea that interface engineering is an effective approach for managing cavitation-induced instabilities in thin-film lubrication.

Zhang [37] examined the material characteristics of wall slippage, emphasizing that successful slip necessitates surfaces exhibiting minimal fluid adhesion and strong compressive strength. The current simulation presupposes an ideal slip boundary; in reality, achieving such performance would rely on coating materials or surface patterns that can sustain this equilibrium, as suggested by Zhang [37].

The LCC behavior shown herein reinforces Zhang's theoretical and empirical findings. Zhang [20] forecasted that boundary slip may significantly enhance bearing load when implemented in areas conducive to fluid entrainment, however Zhang [21] illustrated that load augmentation is optimized when slip encompasses a considerable portion of the inlet region, excluding the entire contact zone. The slip-before-pocket design in the present investigation resulted in a maximum LCC increase of 47.76% at H_{min} 15 μm, closely aligning with Zhang's stated enhancement range. In contrast, the slip-on-pocket arrangement consistently diminished LCC; corroborating Zhang's finding that slip in the primary load-supporting region undermines Poiseuille pressure generation. This suggests that the positioning of the slip, rather than its amount, predominantly influences bearing efficiency.

Zhang [27] also noted that slippage, although advantageous for minimizing friction, may compromise the stability of the hydrodynamic film if the shear strength at the interface is insufficient. Our findings corroborate that analysis: the combined-slip configuration enhanced performance solely within specific film thickness ranges, indicating that an excessively broad slip zone undermines film stiffness. The findings generally indicate that regulated partial slip, particularly at the inlet, enhances both load and film stability, while excessive slip coverage results in declining or negative benefits.

Zhang [37] emphasized the necessity of creating surface materials capable of modulating wall slippage from a design perspective. The present findings corroborate that recommendation: the application of slip coatings or hydrophobic micro-textures in specific areas (prior to the pocket) may replicate the predicted performance enhancements in actual systems in industries. Inappropriate or non-uniform coatings may result in uneven pressure and localized film failure. Consequently, subsequent research should empirically assess potential materials with quantifiable interfacial shear strength to realize the controllable slippage proposed by Zhang.

4. CONCLUSION

The CFD modeling has been performed for hydrodynamic circumferential pocket bearing, which are defined by a constant pocket depth of 30 μm and varying minimum lubricant film thicknesses between 15 and 80 μm. Four distinct slip designs were utilized to evaluate the pressure distribution and load-carrying capacity (LCC) in both cavitation and non-cavitation conditions. The following are the conclusions.

1. The maximum pressure across all slip configurations (no-slip, slip-before-pocket, slip-on-pocket, and combined-slip) occurred at H_{min} 15 μm, while the minimum pressures were observed at H_{min} 80 μm. The slip-before-pocket arrangement consistently generated the highest pressure across all thickness levels. The peak pressure attained was 5.09 MPa, noted at H_{min} 15 μm prior to pocket conditions under slip.
2. The LCC exhibited a close alignment with the pressure distribution. The highest LCC values for all slip configurations were recorded at H_{min} 15 μm, whereas the lowest values were noted at H_{min} 80 μm. The slip-before-pocket configuration demonstrated consistently superior performance across all configurations, achieving the highest LCC of 1744.61 N.
3. Comparing cavitation and no cavitation simulations reveals that the no cavitation condition produced higher pressure and LCC values for all slip configurations, unlike the cavitation condition. Cavitation disrupts the continuity of lubricant flow and reduces pressure accumulation, thereby negatively impacting thrust bearing performance.

Future simulations should incorporate many pocket depths for comparative analysis, as this article exclusively investigates a singular pocket depth value from previous research. Experiments are crucial for the accurate validation of research, including the implementation of surface coatings to establish slip conditions.

Acknowledgment

This study received funding from the Ministry of Higher Education, Science, and Technology of the Republic of Indonesia via the Higher Education Service Institution (LLDIKTI) Region VI and the Institute for Research and Community Service (LPPM) of Universitas Wahid Hasyim, under the Regular Fundamental Research scheme, with contract numbers 07/LP2M-UWH/PFR/V/2025.

REFERENCES

[1] B. J. Hamrock, S. R. Schmid, and B. O. Jacobson, *Fundamentals of Fluid Film Lubrication*, 0 ed. CRC Press, 2004. doi: 10.1201/9780203021187.

[2] Z. Song, F. Guo, Y. Liu, S. Hu, X. Liu, and Y. Wang, “Investigation of slip/no-slip surface for two-dimensional large tilting pad thrust bearing,” *Industrial Lubrication and Tribology*, vol. 69, no. 6, pp. 995–1004, Oct. 2017, doi: 10.1108/ilt-06-2017-0152.

[3] C. Huang and Y. Zhang, “Multiscale hydrodynamics in thrust bearing involving surface roughness,” *Continuum Mechanics and Thermodynamics*, vol. 36, no. 3, pp. 445–458, Jan. 2024, doi: 10.1007/s00161-023-01275-z.

[4] X. Yu, G. Shi, W. Gao, and X. Yang, “Effect of surface square textures on the physical field of static and dynamic pressure thrust bearings and multi-objective optimization,” *Industrial Lubrication and Tribology*, vol. 76, no. 10, pp. 1294–1307, Oct. 2024, doi: 10.1108/ilt-06-2024-0198.

[5] D. Gropper, L. Wang, and T. J. Harvey, “Hydrodynamic lubrication of textured surfaces: A review of modeling techniques and key findings,” *Tribology International*, vol. 94, pp. 509–529, Oct. 2015, doi: 10.1016/j.triboint.2015.10.009.

[6] D. Sirohi and S. Aggarwal, “Numerical and Experimental Studies on performance Enhancement of thrust pad bearing employing surface texture: a review,” *Tribology in Industry*, vol. 45, no. 3, pp. 542–560, Sep. 2023, doi: 10.24874/ti.1463.03.23.06.

[7] N. Z. Rasep, N. M. N. A. W. M. Yazid, N. S. Samion, and N. nor A. C. Sidik, “Potential of RBD Palm Oil as a Lubricant in Textured Journal Bearing using CFD with Consideration of Cavitation and Conjugate Heat Transfer,” *CFD Letters*, vol. 14, no. 2, pp. 98–110, Mar. 2022, doi: 10.37934/cfdl.14.2.98110.

[8] Y. Chen, H. Wang, X. Wang, C. Yu, Y. Sun, and J. Feng, “Performance analysis and geometrical design of Spiral-Grooved thrust bearing employing CFD model,” *Journal of the Institution of Engineers (India) Series C*, vol. 102, no. 3, pp. 765–775, Apr. 2021, doi: 10.1007/s40032-021-00689-5.

[9] D. G. Fouflias, A. G. Charitopoulos, C. I. Papadopoulos, L. Kaiktsis, and M. Fillon, “Performance comparison between textured, pocket, and tapered-land sector-pad thrust bearings using computational fluid dynamics thermohydrodynamic analysis,” *Proceedings of the Institution of Mechanical Engineers Part J Journal of Engineering Tribology*, vol. 229, no. 4, pp. 376–397, Sep. 2014, doi: 10.1177/1350650114550346.

[10] M. Muchammad, M. Tauviqirrahman, Y. M. Rizki, I. Syafaat, F. Maharani, and M. I. Ammarullah, “Elastohydrodynamic analysis of multistep texture effects and partial surface roughness on the tribological performance of steel journal bearings,” *Discover Applied Sciences*, vol. 7, no. 4, Apr. 2025, doi: 10.1007/s42452-025-06789-6.

[11] M. Omar, Y. Abdelkader, M. Fatouma, and M. Kouider, “Parametric Design optimization of convergent textured thrust bearing in THD behaviour,” *Tribology in Industry*, vol. 45, no. 4, pp. 650–663, Dec. 2023, doi: 10.24874/ti.1497.06.23.09.

[12] I. Syafaat *et al.*, “The synergistic influence of texture and slip formations in hydrodynamic thrust bearings on tribological characteristics,” *Results in Engineering*, vol. 21, p. 101779, Jan. 2024, doi: 10.1016/j.rineng.2024.101779.

[13] T. Ibatan, Uddin, and M. A. K. Chowdhury, “Recent development on surface texturing in enhancing tribological performance of bearing sliders,” *Surface and Coatings Technology*, vol. 272, pp. 102–120, Apr. 2015, doi: 10.1016/j.surfcoat.2015.04.017.

[14] Y. Chen, X. Shi, X. Wang, H. Wang, C. Yu, and Y. Sun, “Multi-objective analysis design of spiral groove conical bearing considering cavitation effects,” *Results in Engineering*, vol. 15, p. 100582, Aug. 2022, doi: 10.1016/j.rineng.2022.100582.

[15] B. A. Abass, S. Y. Ahmed, and Z. H. Kadhim, “Analysis and Optimization of Nanolubricated Journal Bearing under Thermoelasto-Hydrodynamic Lubrication Considering Cavitation Effect,” *Tribology in Industry*, vol. 45, no. 4, pp. 618–633, Dec. 2023, doi: 10.24874/ti.1441.01.23.04.

[16] M. R. Hameed and S. A. Ali, “Dynamic and Thermal Performance Analysis of Textured Bearings with TiO2 Nanoparticles,” *Tribology in Industry*, vol. 47, no. 7, pp. 23–39, Mar. 2025, doi: 10.24874/ti.1742.08.24.12.

[17] N. A. Androva, N. M. Tauviqirrahman, N. N. Sinaga, N. M. Khafidh, N. M. Sagaf, and N. Hafid, “A Comparative Study on Hydrodynamic Analysis with and without Cavitation Modelling: A Study on Textured Slip Journal Bearing,” *CFD Letters*, vol. 16, no. 8, pp. 48–63, Apr. 2024, doi: 10.37934/cfdl.16.8.4863.

[18] Z. Wu, X. Ding, L. Zeng, X. Chen, and K. Chen, “Optimization of hydrodynamic lubrication performance based on a heterogeneous slip/no-slip surface,” *Industrial Lubrication and Tribology*, vol. 71, no. 6, pp. 772–778, Apr. 2019, doi: 10.1108/ilt-07-2018-0268.

[19] I. Syafaat, M. A. Shobirin, A. Nugroho, N. Muchammad, M. Tauviqirrahman, and B. Setiyana, "The effect of boundary slip condition on cavitation reduction in a closed pocket hydrodynamic thrust bearing," *AIP Conference Proceedings*, vol. 3250, p. 080002, Jan. 2025, doi: 10.1063/5.0240610.

[20] Y. Zhang, "Boundary slippage for improving the load and friction performance of a step bearing," *Transactions of the Canadian Society for Mechanical Engineering*, vol. 34, no. 3–4, pp. 373–387, Sep. 2010, doi: 10.1139/tcsme-2010-0022.

[21] Y. Zhang, "A tilted pad thrust slider bearing improved by the boundary slippage," *Meccanica*, vol. 48, no. 4, pp. 769–781, Oct. 2012, doi: 10.1007/s11012-012-9630-6.

[22] N. I. Syafaat *et al.*, "Numerical study of comparison of thrust bearing slip - no slip condition on acoustic performance," *CFD Letters*, vol. 15, no. 9, pp. 1–17, Aug. 2023, doi: 10.37934/cfdl.15.9.117.

[23] J. H. Choo, R. P. Glovnea, A. K. Forrest, and H. A. Spikes, "A low friction bearing based on liquid slip at the wall," *Journal of Tribology*, vol. 129, no. 3, pp. 611–620, Jan. 2007, doi: 10.1115/1.2736704.

[24] M. Tauviqirrahman, A. Pratama, J. Jamari, and M. Muchammad, "Hydrodynamic lubrication of textured journal bearing considering slippage: Two-dimensional CFD analysis using multiphase cavitation model," *Tribology in Industry*, vol. 41, no. 3, pp. 401–415, Sep. 2019, doi: 10.24874/ti.2019.41.03.10.

[25] H. K. Versteeg and W. Malalasekera, *An introduction to computational fluid dynamics: the finite volume method*, 2. ed., [Nachdr.]. Harlow: Pearson/Prentice Hall, 2007.

[26] G. H. Schnerr and J. Sauer, "Physical and numerical modeling of unsteady cavitation dynamics," in *Proceeding of the 4th International Conference on Multiphase Flow (ICMF-2001)*, 2001, vol. 1, no. June, pp. 1–12.

[27] Y. Zhang, "Review of Hydrodynamic Lubrication with Interfacial Slippage," *Journal of the Balkan Tribological Association*, vol. 20, no. 4, pp. 522–538, 2014.

[28] V. Zouzoulas and C. I. Papadopoulos, "3-D thermohydrodynamic analysis of textured, grooved, pocketed and hydrophobic pivoted-pad thrust bearings," *Tribology International*, vol. 110, pp. 426–440, Oct. 2016, doi: 10.1016/j.triboint.2016.10.001.

[29] M. Chalkiopoulos, A. Charitopoulos, M. Fillon, and C. I. Papadopoulos, "Effects of thermal and mechanical deformations on textured thrust bearings optimally designed by a THD calculation method," *Tribology International*, vol. 148, p. 106303, Mar. 2020, doi: 10.1016/j.triboint.2020.106303.

[30] G. Koutsoumpas, A. Charitopoulos, C. I. Papadopoulos, and M. Fillon, "Computational evaluation of dynamic coefficients of thrust bearings; effect of artificial texturing on thermohydrodynamic performance," *Surface Topography Metrology and Properties*, vol. 8, no. 2, p. 024009, May 2020, doi: 10.1088/2051-672x/ab8ffb.

[31] ANSYS, *ANSYS Fluent, Version 16.0: User Manual*. Canonsburg, USA: ANSYS Inc., 2017.

[32] I. Syafaat, N. Rizqi, N. Muchammad, M. Tauviqirrahman, and B. Setiyana, "CFD analysis of hydrodynamically lubricated textured slider bearings," in *Lecture notes in mechanical engineering*, pp. 377–380, 2022, doi: 10.1007/978-981-19-3179-6_70.

[33] I. Syafaat, M. Nurkhafidin, M. Muchammad, M. Tauviqirrahman, and B. Setiyana, "Effect of Reynolds number on pressure behavior of slider contact with triangular dimple considering slip," *Materials Today Proceedings*, vol. 63, pp. S273–S275, Jan. 2022, doi: 10.1016/j.matpr.2022.02.458.

[34] M. Tauviqirrahman, J. Jamari, B. S. Wibowo, H. M. Fauzan, and M. Muchammad, "Multiphase computational fluid dynamics analysis of hydrodynamic journal bearing under the combined influence of texture and slip," *Lubricants*, vol. 7, no. 11, p. 97, Oct. 2019, doi: 10.3390/lubricants7110097.

[35] I. Syafaat *et al.*, "A 3D design of the hydrodynamic pocketed thrust bearing with slip engineered for eliminating cavitation," *Results in Engineering*, vol. 24, p. 103039, Oct. 2024, doi: 10.1016/j.rineng.2024.103039.

[36] M. Muchammad, M. Tauviqirrahman, J. Jamari, and D. J. Schipper, "An analytical approach on the tribological behaviour of pocketed slider bearings with boundary slip including cavitation," *Lubrication Science*, vol. 29, no. 3, pp. 133–152, Nov. 2016, doi: 10.1002/ls.1361.

[37] Y. Zhang, "Can Any Material Accommodate the Control of Wall Slippage?," *Journal of the Balkan Tribological Association*, vol. 20, no. 2, pp. 309–320, Nov. 2014.